Simple Noninvasive Quantification Method for Measuring Myocardial Glucose Utilization in Humans Employing Positron Emission Tomography and Fluorine-18 Deoxyglucose

Sanjiv S. Gambhir, Markus Schwaiger*, Sung-Cheng Huang, Janine Krivokapich, Heinrich R. Schelbert, Christoph A. Nienaber, and Michael E. Phelps

Division of Nuclear Medicine and Biophysics, Department of Radiological Sciences, and Laboratory of Nuclear Medicine, Department of Biomathematics, Division of Cardiology, Department of Medicine, UCLA School of Medicine, Los Angeles, California

To estimate regional myocardial glucose utilization (rMGU) with positron emission tomography (PET) and 2-[^{18}F]fluoro-2-deoxy-D-glucose (FDG) in humans, we studied a method which simplifies the experimental procedure and is computationally efficient. This imaging approach uses a blood time-activity curve derived from a region of interest (ROI) drawn over dynamic PET images of the left ventricle (LV), and a Patlak graphic analysis. The spillover of radioactivity from the cardiac chambers to the myocardium is automatically removed by this analysis. Estimates of rMGU were obtained from FDG PET cardiac studies of six normal human subjects. Results from this study indicate that the FDG time-activity curve obtained from the LV ROI matched well with the arterial plasma curve. The rMGU obtained by Patlak graphic analysis was in good agreement with direct curve fitting results ($r = 0.90$). The average standard error of the estimate of the Patlak rMGU was low (3%). These results demonstrate the practical usefulness of a simplified method for the estimation of rMGU in humans by PET. This approach is noninvasive, computationally fast, and highly suited for developing parametric images of myocardial glucose utilization rate.

J Nucl Med 30:359–366, 1989

With the recent development of high spatial and temporal resolution positron emission tomography (PET) scanners, it has become possible to quantify more accurately regional myocardial tissue concentrations of 2-[^{18}F]fluoro-2-deoxy-D-glucose (FDG). The use of FDG for PET imaging of the heart was first introduced in 1978 by Phelps et al. (*1*). Studies in rats, dogs, monkeys, and humans (*1–5*) suggested that FDG could be used to measure the rate of exogenous glucose utilization in the heart. PET imaging with FDG and nitrogen-13 ammonia (a blood flow tracer) has been shown to be useful for identifying myocardial ischemia and defining tissue viability in patients with ischemic heart disease (*6–9*). Most of these studies relied on qualitative evaluation of regional FDG uptake and its relationship to flow. To exploit fully the quantitative capabilities of PET, a simple tracer-kinetic method is needed to measure regional glucose utilization.

A three-compartment FDG tracer kinetic model was first developed for cerebral tissues by Sokoloff et al. (*10*) as applied to the autoradiographic method. This model was subsequently extended (*11,12*), and used for estimating local cerebral metabolic rate for glucose utilization in man with PET. The FDG model has also been validated in the isolated, arterially perfused rabbit septum (*13,14*), with the estimated utilization rates for exogenous glucose correlating well with those derived by the Fick method under a wide range of perfusion and workload conditions. In addition, the FDG model has been validated in canine myocardium by comparison with the Fick method (*15*).

In previous studies, quantitation of regional myocar-

Received Apr. 29, 1988; revision accepted Oct. 27, 1988.

For reprints contact: S.C. Huang, DSc, Div. of Nuclear Medicine and Biophysics, UCLA School of Medicine, Los Angeles, CA 90024.

*Present address: Div. of Nuclear Medicine, Dept. of Internal Medicine, University of Michigan Medical School, Ann Arbor, Michigan.

dial glucose utilization (rMGU) by PET imaging has been complicated by several factors: (a) the limited spatial and temporal resolution of PET scanners; (b) the spillover of radioactivity from the blood pool to the tissue pool at early times, and the spillover from the tissue to the blood pool at later times, thus complicating the blood and tissue time-activity curves obtained from PET images; (c) slow convergence in fitting for the rate constants of the FDG model, due to noise levels encountered in these dynamic studies; and (d) the invasiveness of arterial blood sampling in humans to obtain the blood time-activity curves.

The purpose of this study was to develop and validate a simplified PET approach which does not have the above limitations. We have used a blood time-activity curve derived from regions of interest (ROIs) drawn in the left ventricle (LV) of PET images, and a Patlak graphic analysis to obtain estimates of rMGU. This Patlak analysis has been compared to standard nonlinear regression (curve fitting).

MATERIALS AND METHODS

Preparation of FDG

FDG was synthesized by the method described previously by Hamacher et al. (*16*). The specific activity was 5 Ci/mg. The radiochemical purity was >99%.

Human Subjects and Blood Sampling

Six normal human volunteers (18–32 yr of age) were enrolled in this study. The study protocol had been approved by the UCLA Human Subject Protection Committee. Each volunteer had a carbohydrate-containing meal 2–3 hr before the study. Ten millicuries of FDG were injected intravenously with an infusion pump over a 15–30 sec interval. Starting ~10 sec after the injection of FDG, arterial samples from an arterial line were withdrawn every 15–20 sec for ~5 min, and then every 1 min for the next 10 min. The sampling interval was then increased steadily during the rest of the study. To define the time course of equilibration of ^{18}F activity between red blood cells and plasma, selected blood samples were divided into two aliquots. Fluorine-18 activity in the whole blood and in the plasma was measured in a well counter and corrected for radioactive decay. Plasma glucose concentrations were measured at the beginning and end of the study using standard enzymatic techniques (*17*).

Image Acquisition

The volunteers were studied using an ECAT III PET scanner (CTI, Corp. Knoxville, TN) with three imaging planes (*18*). For all studies, acquisition of transmission images was performed for correction of photon attenuation prior to obtaining the PET emission images. Forty-six dynamic scans were obtained in 117 min using the following protocol: twelve 10-sec, ten 30-sec, ten 120-sec, ten 300-sec, and four 600-sec scans.

Calibration and Image Processing

To obtain a calibration factor relating tomographic measurement of myocardial activity to blood sample activity obtained from the well counter, a cylindrical phantom (20 cm diameter) containing ^{18}F was scanned after each study. A known volume of activity from the cylinder was also counted in the well counter. This provided the calibration between cts/min/pixel from the PET images and cts/min/ml obtained from the well counter.

The cross-sectional images were reconstructed to give a spatial resolution of 13.5 mm full width at half maximum, and all images were corrected for the physical decay of ^{18}F to the FDG injection time. Myocardial tissue time-activity curves were obtained as follows. For each study two to three planes were analyzed with six myocardial ROIs defined per plane. The ROIs were drawn on the last image of the dynamic scan and then applied to all previous images. Two elliptical ROIs were placed on the septum, and two elliptical ROIs were placed on the free wall. The elliptical ROIs were placed so that they were away from the apparent tissue edge of the myocardium in order to minimize noise in the tissue curves due to patient movement as well as heart motion. One ROI was drawn around the whole free wall and one around the whole myocardium. Finally, a circular ROI (0.7–1.2 cm diameter) was drawn in the LV chamber of the middle plane to obtain the LV time-activity curve. Counts/pixel were obtained from the ROIs, and these values were converted to cts/pixel/min by normalizing for the acquisition time of the image. These values were finally converted to equivalent well counter cts/ml/min using the calibration factor.

Corrections Applied to Time-Activity Curves

All time-activity curves were corrected for the effects of dead time of the scanner (*19*). In order to correct for the partial-volume effect associated with object size (*20*), recovery coefficients (RC) obtained experimentally from phantom studies were used. A standard myocardial wall thickness of 1.2 cm (RC = 0.70) was assumed in correcting the partial-volume effect in myocardial time-activity curves. The true myocardial tissue activity was calculated as the observed tracer concentration divided by the RC. The LV curve was corrected for spillover from myocardial tissue to LV at later times using the spillover fraction from myocardium to blood (calculated as the difference in activity between the arterial and LV curve at the last sampled point divided by the average activity at this time in the whole myocardium).

Calculation of rMGU

The three-compartment FDG tracer-kinetic model depicted in Figure 1 was used in the present study. The differential equations governing the model have been described previously (*11,12*). Regional myocardial glucose utilization rate can be calculated as $rMGU = (C_p/LC) \times (k_1 \times k_3/(k_2 + k_3))$. C_p is the plasma concentration of glucose; LC is the lumped constant that accounts for differences in the transport and phosphorylation of FDG and glucose (*10,11,12*). For this study, LC was assumed to be a constant equal to 0.67 (*15*). The values of the rate constants were obtained by fitting the FDG model (using the arterial FDG curve as the input function) to the measured tissue time-activity curves. The fit was done using a least squares nonlinear regression to fit for the rate constants k_1–k_4 and the spillover fraction. The fitting of the spillover fraction as a fifth parameter added to the model is an approach similar to that used in brain FDG studies to account for the FDG in the blood volume (*21*).

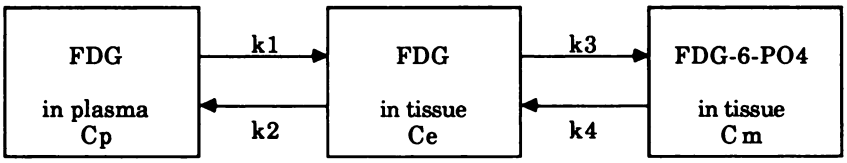

FIGURE 1
Three-compartment tracer kinetic model for FDG. Terms C_p, C_e, and C_m are, respectively, FDG concentration in plasma, FDG concentration in tissue, and FDG-6-PO_4 concentration in tissue. The rate constants k_1–k_4 govern the rate of exchange of material between compartments.

The second approach applied to the image data to estimate rMGU employed the Patlak graphic analysis. This technique, usable for general models in which the tracer is irreversibly trapped in a system, was first proposed and described by Patlak et al. (*22,23*). In this study we have used this analysis technique to estimate rMGU. A similar technique for estimating rMGU has been suggested previously by Araujo (personal communication). Equation (1) is the basic equation of the Patlak analysis as applied to the FDG model.

$$A_m(t)/C_p(t) = [(k_1 \times k_3)/(k_2+k_3)]/C_p(t) \times \int_0^t C_p(s)\,ds + W. \quad (1)$$

The dephosphorylation rate constant (k_4) of FDG has been assumed to be zero. $A_m(t)$ is the tissue activity at time t, $C_p(t)$ is the plasma activity at time t, and W is a function of the steady-state volume of the reversible compartments and the effective plasma volume. A plot of $A_m(t)/C_p(t)$ vs. $\int C_p(s)\,ds/C_p(t)$ should have a linear relationship at late times with slope $= K = (k_1 \times k_3)/(k_2 + k_3)$, and a y intercept equal to W. Thus, this graphic approach permits the calculation of rMGU by giving a direct estimate of K from the slope of the linear relationship on the plot.

Because the Patlak analysis assumes that the tracer is irreversibly trapped in the system ($k_4 = 0$ in the FDG model), simulations were performed to examine the effects of $k_4 > 0$ on the Patlak analysis. Using as an input function the LV time-activity curve from a study, the response of the FDG model was obtained for various values of the rate constants k_1–k_4 and the spillover fraction. From these simulations, the effect of a nonzero k_4 on the Patlak plot was determined, and a multiplicative correction factor, which is a function of k_4, was derived to adjust the points on the Patlak plot before applying a linear regression to obtain the slope K. This correction factor was calculated by determining the deviation of a given point on the Patlak plot for various values of $k_4 > 0$ from the corresponding data point for $k_4 = 0$. The correction factor was determined from the input functions of each of the patient's studies and an average value was used. The percent difference between the highest and lowest values was 4%.

To calculate rMGU from the Patlak analysis the following procedure was used: an estimate of k_4 was first obtained by fitting the model to the tissue time-activity curve of the whole myocardial region (using as an input function the arterial plasma time-activity curve). The k_4 value so obtained was then used to calculate a correction factor for all regions within that particular plane. The tissue activity at three separate time points (t = 12, 35, 55 min) were used to estimate the slope K. These time points were chosen so as to allow for the possibility of moving to different planes between the selected time points during the acquisition protocol, while still maintaining adequate sampling of the Patlak curve for the proper estimation of rMGU. To assess the possibility of further simplification of the experimental protocol, the use of only two tissue points (t = 12, 35 min) to estimate the slope K was also investigated.

To compare the estimates of rMGU based on the arterial plasma input function to those based on the LV input function, the Patlak analysis (with three tissue points) was repeated using the LV time-activity curve as the input function.

RESULTS

The whole-blood time-activity curve versus the plasma time-activity curve from a typical study is illustrated in Figure 2. Note that the whole-blood and plasma radioactivities reach equilibrium very quickly, thus justifying the use of either the whole blood or the plasma time-activity curve as the input function. Serial

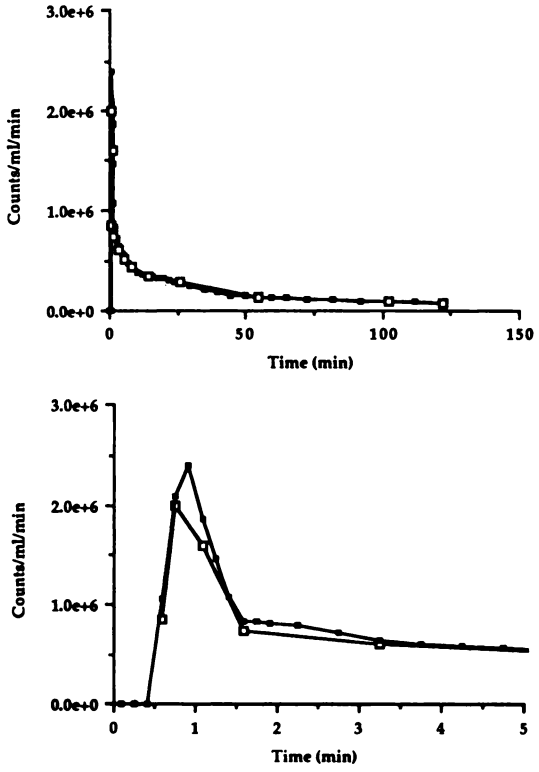

FIGURE 2
Upper: ^{18}F radioactivity in plasma (■) and whole blood (□). The peak region is expanded in the lower graph. The whole-blood activity is less than the plasma initially, but an equilibrium is reached very rapidly.

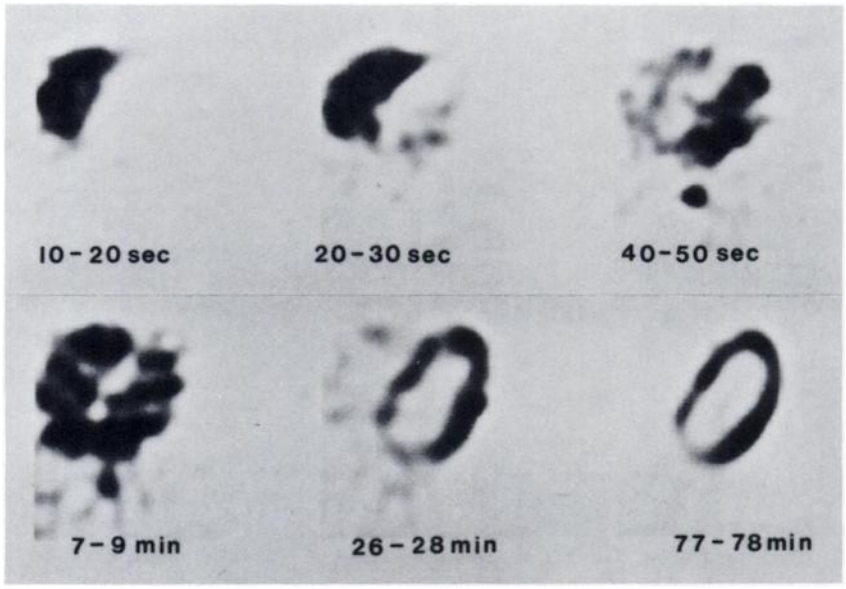

FIGURE 3
FDG radioactivity images obtained from a typical dynamic study. The activity is first primarily in the right ventricle (10–20 sec, 20–30 sec) and then it shifts to the left ventricle (40–50 sec). Activity is seen in the ventricles and the myocardium tissue (7–9 min), and primarily in the myocardium tissue in the later images (26–28 min, 77–87 min). It is from these images that the time-activity curves for LV blood-pool and myocardial tissue were obtained.

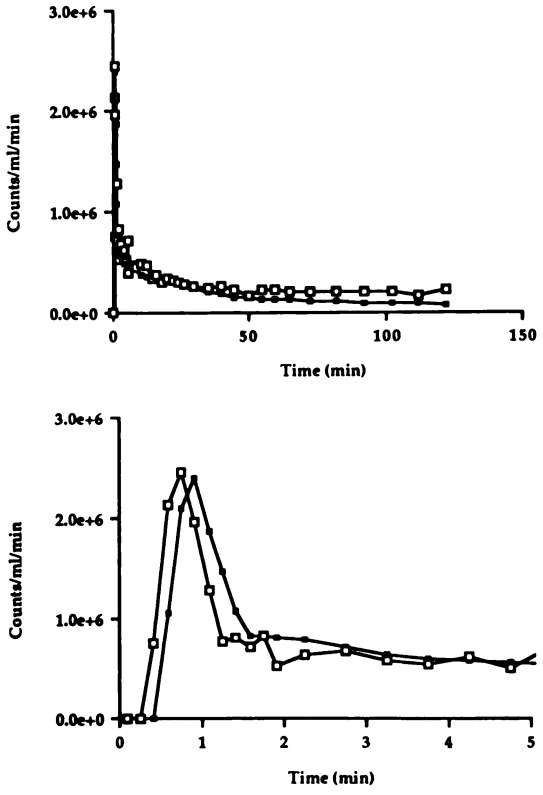

FIGURE 4
Upper: Plasma (solid squares) and LV blood pool (open squares) FDG time-activity curves. The LV curve was not corrected for spillover from the tissue to the LV at later times. This results in the overestimation of activity in the blood pool as compared to the plasma curve for times >~45 min. The peak region is expanded on the lower graph. The differences in the peaks are partly due to delay and dispersion of tracer as it travels from LV to the radial artery, and partly because of differences in radioactivity in whole blood vs. plasma.

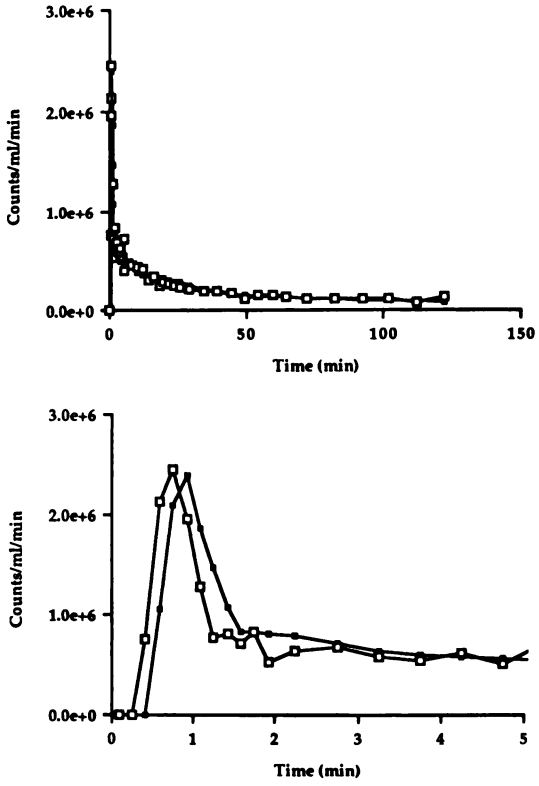

FIGURE 5
Upper: Plasma (solid squares) and corrected LV blood pool (open squares) FDG time-activity curves. The LV curve is corrected for the effects of spillover from tissue to the LV and agrees well with the arterially sampled plasma curve. The peak region is expanded in the lower graph.

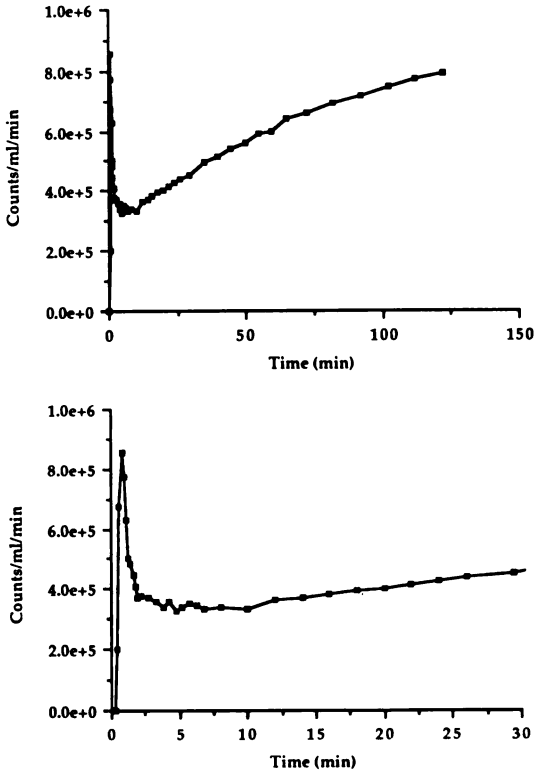

FIGURE 6
Upper: Tissue time-activity curve obtained from an elliptical ROI drawn in the free wall. The early peak (0–2 min) is the result of spillover of radioactivity from LV blood pool to the tissue. The peak region is expanded on the lower graph.

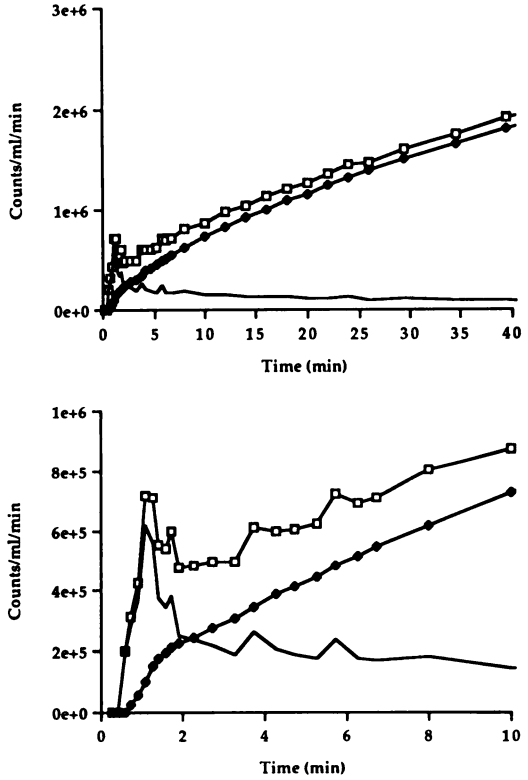

FIGURE 7
Upper: Measured regional tissue time-activity curve (open squares) from a ROI drawn around the whole myocardium, fitted tissue curve (solid diamonds), and the spillover fraction (solid line without symbols). The fitted tissue curve was produced by fitting for rate constants k_1–k_4 and the spillover fraction. A smooth tissue time-activity curve results after correcting for the effects of spillover from the LV blood pool to the tissue. The peak region is expanded on the lower graph.

FDG images obtained from one study are shown in Figure 3. The radioactivity first appears in the right ventricle, followed by the left ventricle, and then in the myocardial tissue as a function of time.

Comparisons of the plasma and the LV time-activity curves are illustrated in Figure 4. The LV curve is not corrected for spillover from tissue back to LV which accounts for the overestimation of radioactivity measured in the blood pool as compared to the plasma curve for times >~45 min. A difference in the peaks of the plasma curve and the LV curve were noted. This is likely due to the delay and dispersion of the tracer as it travels from the left ventricle to the radial artery, where samples for the plasma time-activity curve were obtained, and due to the difference between whole-blood and plasma radioactivities. Plasma and spillover-corrected LV curves (Fig. 5) agree very well except near the peak, where delay and dispersion have the most pronounced effects.

A tissue time-activity curve from a whole myocardial ROI applied to a sequence of images from a dynamic scan is illustrated in Figure 6. The observed myocardial tissue time-activity curve contains spillover from LV blood pool to tissue (seen as the early peak from 0–2 min). An example of the measured regional tissue time-activity curve, the fitted tissue curve (via nonlinear regression) and the spillover fraction are shown in Figure 7. Note that there is a continuous rise in radioactivity in the tissue when the effects of spillover are accounted for in the model.

Simulation of the effect of changing k_4 on the Patlak plot revealed that as k_4 got larger the departure from linearity increased and therefore the magnitude of the correction factor increased (Fig. 8). The correction factor was found to be insensitive to the exact values of k_1–k_3 used. The spillover fraction from LV to myocardium only affected the y intercept of the Patlak plot and not the slope. Thus, the effects of spillover are automatically removed in this graphical analysis.

Results of the estimates of rMGU obtained by microparameter regression (with the plasma input function) and those by the Patlak analysis (with the plasma and LV input functions) with three tissue points are shown in Table 1. These data represent the mean ± s.d. over all ROIs used for each subject. The rMGU values obtained by the two data analysis techniques while using the plasma input function are in good agreement ($r = 0.90$) as shown in Figure 9. The average standard error

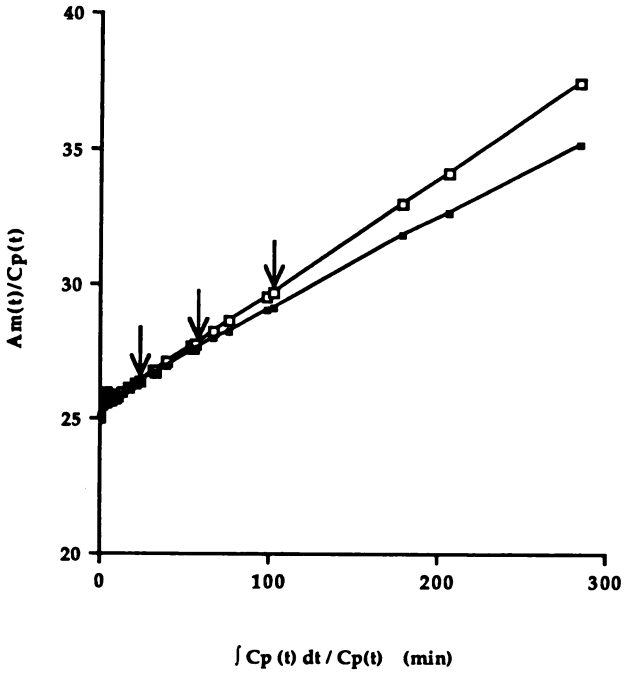

FIGURE 8
Patlak plot with $k_4 = 0$ (open squares) and $k_4 = 0.005$ (solid squares) min^{-1}. Note that for $k_4 > 0$ the plot becomes nonlinear. The three arrows represent the three tissue points chosen in this study for estimating rMGU. A correction based on k_4 was applied to these points before estimating the slope by linear regression.

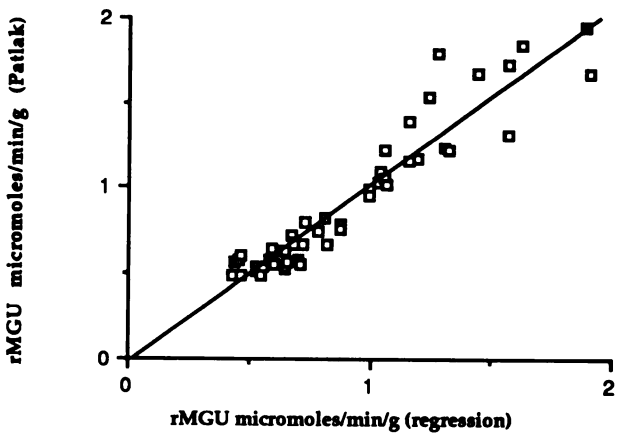

FIGURE 9
Plot of rMGU values as obtained by Patlak and nonlinear regression (using the plasma input function), over all regions from the six patients studied in which the nonlinear regression converged. There is good agreement (r = 0.90) between estimates by the two techniques.

of the Patlak rMGU is 3%. The use of only two tissue points in the Patlak analysis gave results which did not correlate as well with the microparameter regression (r = 0.80). Also, rMGU as obtained by Patlak analysis for both the plasma and LV input functions are in good agreement (r = 0.94), thus validating the use of the LV input function. Results from the microparameter regression indicate that the dephosphorylation rate constant (k_4) of FDG-6-PO4 in myocardium averaged over all regions and all patients studied is 0.006 ± 0.003 min^{-1}.

TABLE 1
rMGU Estimates

Study no.	rMGU (Regression) Plasma input function	rMGU (Patlak) Plasma input function	rMGU (Patlak) LV input function
1	0.93 ± 0.22*	0.97 ± 0.24	0.93 ± 0.22
2	0.61 ± 0.21	0.72 ± 0.23	0.73 ± 0.22
3	0.62 ± 0.10	0.65 ± 0.10	0.56 ± 0.06
4	1.15 ± 0.13	0.99 ± 0.10	1.11 ± 0.12
5	0.72 ± 0.10	0.80 ± 0.11	0.70 ± 0.09
6	1.52 ± 0.28	1.51 ± 0.22	1.58 ± 0.26

* Mean ± s.d. for each patient in μmol/min/g.

DISCUSSION

Clinical FDG study protocols for humans require a fast, noninvasive, quantitative analysis technique that will produce reliable estimates of rMGU. In the present study it is demonstrated that the Patlak analysis approach can satisfy the requirements, if the partial volume, bi-directional spillover, and dephosphorylation ($k_4 > 0$) are properly taken into account.

The correction for the partial-volume effect could potentially be improved by using recovery coefficients based on regional assessment of myocardial wall thickness which can be measured with echocardiography. The use of the RC affects both the Patlak analysis and the microparameter regression in the same way, and thus the use of RC is not a limitation unique to the present technique. Another important issue in dynamic cardiac studies is that the cross-contamination of activity between tissue and the vascular space can complicate the quantitation of rMGU. Spillover from the cardiac chambers to tissue is not a problem for the Patlak analysis since this only affects the y intercept and not the slope and thus does not affect the estimates of rMGU. Spillover from tissue to the LV blood pool at late times is a more complicated factor when the LV curve is to be used as an input function. Correcting both the tissue and LV blood-pool time-activity curves for the effects of spillover (from the LV and back to it) based on geometric physical correction can also be performed (*24,25*). However, the spillover to the septum from the right ventricle is not usually accounted for. This is an area which is currently under further investigation.

Included in the present Patlak analysis is the correction for a positive k_4. An estimate of k_4 was obtained from an ROI defining the entire myocardium, and then corections applied to all ROIs within the cross-section. To obtain this estimate for k_4, a high-temporal-resolution tissue time-activity curve over ~120 min is needed. In a protocol where only three tissue scans are performed, one could use a population average k_4 value without significantly increasing the error in the rMGU estimate. The use of only three tissue scan times (t = 12, 35, 55 min) was found to give reliable estimates of rMGU as compared to the use of nonlinear regression. Further simplification in the protocol by using only two tissue scan times (t = 12, 35 min) diminished the correlation with nonlinear regression.

Another important factor affecting the accuracy of rMGU estimates is the noise characteristics inherent to dynamic studies. In addition to statistics, noise can be a result of the movement of the patient within the scanner, and respiratory movement, as well as cardiac motion. All of these noise sources limit the estimation accuracy and frequently prevent nonlinear regression from adequately estimating rMGU. The computational burden of nonlinear regression with the FDG model is nontrivial, and the fit obtained can be relatively poor as the region size decreases. With the Patlak technique, however, estimates of rMGU can be obtained even from noisy data with the added advantage of simple computation.

The Patlak analysis could be used to analyze multiple planes (with a multiplane scanner) as long as each set of planes were imaged for ~10 min and for at least three distinct time intervals. A continuous LV input function can still be obtained in this way because most planes contain part of the LV chamber. Also, some of the noise problems associated with the cardiac motion could be decreased by using gated images and a tomograph with higher spatial resolution (*18*).

In conclusion, this study demonstrates the usefulness of the Patlak method for estimating rMGU utilizing only three scans to obtain the tissue data points, and a blood-pool time-activity curve derived from a ROI drawn in the LV chamber. This approach is noninvasive, computationally fast, and highly suited for developing parametric images of myocardial glucose utilization (i.e., images of rMGU). These images would directly show pixel-by-pixel glucose utilization in myocardial tissue as opposed to pixel-by-pixel ^{18}F activity distribution from which glucose utilization would have to be calculated. Further work is underway to implement the approach to obtain parametric images of myocardial glucose utilization.

ACKNOWLEDGMENTS

The authors thank Ron Sumida, Larry Pang, Cindy Moran, and Francine Aguilar for technical assistance with the studies. They also thank Kirk Mahoney for his comments on the manuscript.

REFERENCES

1. Phelps ME, Hoffman EJ, Selin CE, et al. Investigation of [^{18}F]2-fluoro-2-deoxyglucose for the measurement of myocardial glucose metabolism. *J Nucl Med* 1978; 19:1311–1319.
2. Phelps ME, Schelbert HR, Hoffman EJ, et al. Physiological tomography studies of myocardial glucose metabolism, perfusion and blood pools with multiple gated acquisition. *Adv Clin Cardiol* 1980; 1:373–393.
3. Schwaiger M, Huang SC, Krivokapich J, et al. Myocardial glucose utilization measured noninvasively in man by positron tomography [Abstract]. *J Am Coll Cardiol* 1983; 1:688.
4. Gallagher BM, Ansari A, Atkins H, et al. Radiopharmaceuticals XXVII. ^{18}F-labeled 2-deoxy-2-fluoro-D-glucose as a radiopharmaceutical for measuring regional myocardial glucose metabolism in vivo: tissue distribution and imaging studies in animals. *J Nucl Med* 1977; 18:990–996.
5. Gallagher BM, Fowler JS, Gutterson NI, et al. Metabolic trapping as a principle of radiopharmaceutical design: some factors responsible for the biodistribution of [^{18}F]2-deoxy-2-fluoro-D-glucose. *J Nucl Med* 1978; 19:1154–1161.
6. Marshall RC, Tillisch JH, Phelps ME, et al. Identification and differentiation of resting myocardial ischemia and infarction in man with positron computed tomography, ^{18}F-labeled fluorodeoxyglucose and N-13 ammonia. *Circulation* 1983; 67:766–777.
7. Brunken R, Tillisch J, Schwaiger M, et al. Regional perfusion, glucose metabolism and wall motion in chronic electrocardiographic Q-wave infarctions. Evidence for persistence of viable tissue in some infarct regions by positron emission tomography. *Circulation* 1986; 73:951–963.
8. Brunken R, Schwaiger M, Grover-McKay M, et al. Positron emission tomography detects tissue metabolic activity in myocardial segments with persistent thallium perfusion defects. *J Am Coll Cardiol* 1987; 10:557–567.
9. Schwaiger M, Brunken R, Grover-McKay M, et al. Regional myocardial metabolism in patients with acute myocardial infarction assessed by positron emission tomography. *J Am Coll Cardiol* 1986; 8:800–808.
10. Sokoloff L, Reivich M, Kennedy C, et al. The [^{14}C] deoxyglucose method for the measurement of local cerebral glucose utilization: theory, procedure, and normal values in the conscious and anesthetized albino rat. *J Neurochem* 1977; 28:897–916.
11. Phelps ME, Huang SC, Hoffman EJ, et al. Tomographic measurement of local cerebral glucose metabolic rate in humans with (18F)2-fluoro-2-deoxy-D-glucose: validation of method. *Ann Neurol* 1979; 6:371–388.
12. Huang SC, Phelps ME, Hoffman EJ, et al. Noninvasive determination of local cerebral metabolic rate of glucose in man. *Am J Physiol* 1980; 238:E69–E82.
13. Krivokapich J, Huang SC, Phelps ME, et al. Estimation of rabbit myocardial metabolic rate for glucose using fluorodeoxyglucose. *Am J Physiol* 1982; 243:H884–H895.
14. Krivokapich J, Huang SC, Selin CE, et al. Fluoro-

deoxyglucose rate constants, lumped constant, and glucose metabolic rate in rabbit heart. *Am J Physiol* 1987; 252:H777–H787.
15. Ratib O, Phelps ME, Huang SC, et al. Positron tomography with deoxyglucose for estimating local myocardial glucose metabolism. *J Nucl Med* 1982; 23:577–586.
16. Hamacher K, Coenen HH, Stöcklin G. Efficient stereospecific synthesis of no-carrier-added 2[^{18}F]-fluoro-2-deoxy-D-glucose using amino polyether supported nucleophilic substitution. *J Nucl Med* 1986; 27:235–238.
17. Bergmeyer H. Methods of enzymatic analysis. Vol 3. New York: Academic Press, 1974:1196–1200.
18. Hoffman EJ, Phelps ME, Huang SC, et al. Dynamic, gated and high resolution imaging with the ECAT III. *IEEE Trans Nuc Sci* 1986; NS-33:452–455.
19. Germano G, Hoffman EJ. An investigation of count rate capability and dead time for a high resolution PET system [Abstract]. *J Nucl Med* 1987; 28:607.
20. Hoffman EJ, Huang SC, Phelps ME. Quantitation in positron emission computed tomography. I. Effect of object size. *J Comput Assist Tomogr* 1979; 3:299–308.
21. Hawkins RA, Phelps ME, Huang SC. Effects of temporal sampling, glucose metabolic rates and disruptions of the blood brain barrier on the FDG model with and without a vascular compartment: studies in human brain tumors with PET. *J Cereb Blood Flow Metab* 1986; 6:170–183.
22. Patlak CS, Blasberg RG, Fenstermacher JD. Graphical evaluation of blood-to-brain transfer constants from multiple-time uptake data. *J Cereb Blood Flow Metab* 1983; 3:1–7.
23. Patlak CS, Blasberg RG. Graphical evaluation of blood-to-brain transfer constants from multiple-time uptake data. Generalizations. *J Cereb Blood Flow Metab* 1985; 5:584–590.
24. Henze E, Huang SC, Rabit O, et al. Measurements of regional tissue and blood-pool radiotracer concentrations from serial tomographic images of the heart. *J Nucl Med* 1983; 24:987–996.
25. Ratib O, Nienaber C, Schelbert HR, et al. Automated quantitative evaluation of gated tomoscintigraphic images. *Circulation* 1987; 76:IV–115.